Title
Enhanced lithium ion transport in garnet-type solid state electrolytes

Journal
Journal of Electroceramics, 38(2-4)

ISSN
1385-3449

Authors
Cheng, Lei
Hou, Huaming
Lux, Simon
et al.

Publication Date
2017-06-01

DOI
10.1007/s10832-017-0080-3

Peer reviewed

Journal of Electroceramics

Enhanced Lithium Ion Transport in Garnet-type Solid State Electrolytes

--Manuscript Draft--

Manuscript Number:	JECR-D-16-00202R1
Full Title:	Enhanced Lithium Ion Transport in Garnet-type Solid State Electrolytes
Article Type:	SI: All Solid State Batteries
Keywords:	All solid state batteries; solid electrolytes; Li7La3Zr2O12; garnet
Corresponding Author:	Marca Doeff -Lawrence Berkeley National Laboratory -Berkeley, CA UNITED STATES
Corresponding Author Secondary Information:	
Corresponding Author's Institution:	-Lawrence Berkeley National Laboratory
Corresponding Author's Secondary Institution:	
First Author:	Marca Doeff
First Author Secondary Information:	
Order of Authors:	Marca Doeff
	Lei Cheng, Ph.D.
	Huaming Hou
	Simon Lux, Ph.D.
	Robert Kostecki, Ph. D.
	Ryan Davis
	Vassilia Zorba, Ph.D.
	Apurva Mehta, Ph.D.
Order of Authors Secondary Information:	
Manuscript Region of Origin:	UNITED STATES
Funding Information:	U.S. Department of Energy (DE-AC02-05CH11231) — Dr. Marca Doeff, Dr. Lei Cheng, Dr. Simon Lux, Dr. Robert Kostecki, Dr. Vassilia Zorba
	U.S. Department of Energy (DE-AC02-76SF00515) — Dr. Ryan Davis, Dr. Apurva Mehta
	National Natural Science Foundation of China (61605161) — Dr. Huaming Hou

Comments to Reviewers:

p. 6, line 29, two independent ?

Typo has been corrected and correction is highlighted in the manuscript.

Figure 4, units on 1/T axis

We have replaced the original with a corrected Figure 4, showing proper units.

I suggest to mention the room T ionic conducitivity values explicitely on p. 10 and to compare them with literature data. I have the impression that the Ar sample is in line with several data sets found in literature and the air sample is worse than average literature data?

We have added several lines on p. 10 giving the room temperature ionic conductivities of the two different samples, along with some extra literature references for Al-substituted LLZO (all highlighted). Reported conductivities vary a great deal depending on processing details, with values ranging from about less than 0.1-0.5 mS/cm^2. The values we report here for LLZO_air are similar to what we reported before for similarly made samples (see reference 25).

Enhanced Lithium Ion Transport in Garnet-type Solid State Electrolytes

Lei Cheng,[1,2] Huaming Hou,[3] Simon Lux,[1] Robert Kostecki, [1] Ryan Davis,[4] Vassilia Zorba,[1] Apurva Mehta,[4] and Marca Doeff[1]

1) Energy Storage and Distributed Resources Division, Lawrence Berkeley National Laboratory, 1 Cyclotron Road, Berkeley, CA 94720 USA

2) Department of Materials Sciences and Engineering, University of California at Berkeley, Berkeley, CA 94720 USA

3) The Peac Institute of Multiscale Sciences, Chengdu, Sichuan 610031, China

4) Stanford Synchrotron Radiation Lightsource, SLAC National Accelerator Laboratory, Menlo Park, CA 94025, USA

Acknowledgments This work was supported by the Assistant Secretary for Energy Efficiency and Renewable Energy, Office of Vehicle Technologies of the U.S. Department of Energy under Contract No. DE-AC02-05CH11231. Use of the Stanford Synchrotron Radiation Lightsource, SLAC National Accelerator Laboratory, is supported by the U.S. Department of Energy, Office of Science, Office of Basic Energy Sciences under Contract No. DE-AC02-76SF00515. The work of Huaming Hou was supported by National Science Foundation of China (grant no. 61605161). Vassilia Zorba acknowledges support from the Chemical Science Division, Office of Basic Energy Sciences of the U.S. Department of Energy under Contract No. DE-AC02-05CH11231. This document was prepared as an account of work sponsored by the United States Government. While this document is believed to contain correct information, neither the United States Government nor any agency thereof, nor the Regents of the University of

Abstract

Al-substituted $Li_7La_3Zr_2O_{12}$ samples processed under argon show enhanced Li-ion transport and interfacial properties in symmetrical cells with lithium electrodes, compared to those prepared in air. In particular, the samples prepared under argon have higher ionic conductivities and lower interfacial impedances in symmetrical lithium cells, and show better DC cycling characteristics. The electronic conductivities are also somewhat higher. Pellets subjected to thermal treatment under the two types of atmospheres have different colors but exhibit similar microstructures. X-ray diffraction experiments suggest that there are slight structural differences between the two types of samples, but few dissimilarities were observed in elemental composition, distribution of ions, oxidation states, or bond lengths using laser-induced breakdown spectroscopy (LIBS), x-ray photoelectron spectroscopy (XPS), and extended x-ray absorption fine structure spectroscopy (EXAFS) to analyze the materials. Additionally, there was no evidence that La or Zr were reduced during the processing under Ar. Possible explanations for the improved electrochemical properties of the sample prepared under Ar compared to the one prepared in air include differences in grain boundary chemistries and conductivities and/or a small concentration of oxygen vacancies in the former.

Keywords: Keywords: All solid state batteries; solid electrolytes; $Li_7La_3Zr_2O_{12}$; garnet

1. Introduction

Ever since initial reports of room temperature ionic conductivities greater than 10^{-4} S/cm, and apparent stability against reduction by lithium [1], interest in the garnet structure $Li_7La_3Zr_2O_{12}$ (LLZO) and variants has intensified greatly [2]. These characteristics suggest that it should be possible to utilize LLZO as a solid electrolyte in solid state [3], [4] [5] or hybrid electrolyte batteries [6, 7] with lithium metal anodes, which may have safety and energy density advantages over conventional Li-ion batteries. Recent work on garnet conductors has been directed towards stabilizing the more conductive cubic polymorph [8, 9] and improving total conductivity via, for example, partial or multiple substitutions [10-14], and/or grain boundary engineering [15-17] [18]. Effort has also been directed towards understanding and improving the interfacial properties [19, 20] and preventing dendrite formation [5, 21] in cells with lithium electrodes. Novel fabrication methods [22] have been used to prepare the thin, dense films of LLZO needed for devices, although this material is notoriously difficult to sinter, and processing variables need to be carefully controlled [23-25]. One variable of interest is the effect of sintering atmosphere on the physical and electrochemical properties of LLZO electrolytes, although only a few studies have been carried out to date [26, 27]. These studies indicate that the atmospheres used during sintering have profound effects on the microstructures and electrochemical properties of the materials, although it is not entirely clear why. For this work, we carried out a comparative study on Al-substituted LLZO sintered under either air or 1.2 atm of Ar. An array of physical and electrochemical techniques were used to characterize the two materials and to determine the origins of the different behaviors that were observed.

2. Experimental

2.1 Powder Synthesis

Stoichiometric amounts of $La(OH)_3$ (CAS# 14507-19-8 Alfa 99.95% REO), ZrO_2(CAS# 1314-23-4 Aldrich 99%) and Li_2CO_3(CAS# 554-13-2 Aldrich >99.0%) were combined with 2% (w/w) Al_2O_3 (Alcoa) and mixed in a zirconia jar for 30 minutes using a Spex Sample Prep 8000M mixer/mill (targeted composition $Li_{6.1}Al_{0.3}La_3Zr_2O_{12}$). The powder mixture was fired at 1000°C for 12 h in a covered alumina tray in static air to form LLZO. The as-synthesized powder was ground by hand and sieved so that particles smaller than 75 μm were produced. Part of the sieved fresh LLZO powder was attrition milled with 2 mm diameter ZrO_2 media in isopropyl alcohol (IPA) at 450 RPM for 2 h, dried in air and used for compacting pellets. The rest of the sieved powder was used as a powder bed without further processing.

2.2 Pellet Preparation

Pellets about 1.5 mm thick were made by cold uniaxial pressing from attrition milled fresh powders using a 3/8 inch stainless steel die without binder. The pressed pellets were placed on alumina trays or a house-made high purity Ni crucible and covered with powder, then fired at 1100°C for 12 h in air or Ar (1.2 atm). Pellets processed in air are designated LLZO_air and those made under Ar are designated LLZO_Ar hereafter. The surfaces of the sintered pellets were dry-polished using several pieces of polishing paper with grit numbers progressing from 400-600. Dry polishing was employed to avoid water contact or contamination from liquid polishing media. An approximately 50 μm thick layer was removed from each surface.

2.3 Characterization

X-ray diffraction (XRD) patterns were obtained on pellets using a Bruker D2-Phaser diffractometer with Cu Kα radiation (λ=1.54 Å). A computed reference pattern for cubic LLZO, using a lattice parameter of 12.972 Å, was constructed using CrystalDiffrac 5.2 (CrystalMaker Software, Ltd) and is used in Figure 3 for comparison purposes. Bulk composition analyses were performed using an inductively coupled plasma optical emission spectrometer (ICP-OES, Perkin-Elmer Optima 5400).

For LIBS measurements, both Nanosecond (ns) laser and Femtosecond (fs) lasers were used to ablate LLZO-Air and LLZO-Ar samples in He gas environment, to avoid interference from the oxygen in air. Laser energies were modified to ensure similar ablation depth per laser pulse. The plasma emission was detected with two independent emission collection and detection systems. In both systems intensified CCDs were used and operated with identical optimized acquisition parameters. Spectral lines with higher lower energy levels were selected in the analyte to avoid self-absorption. Even with two spectra detection systems, not all elements in the samples could be detected at the same time. For the analysis of La, Zr and Li, a ns laser was used for ablation. A high-resolution spectrum detection system was used to detect the La and Zr lines to ensure their lines could be clearly resolved, while a low-resolution spectrum detection system was used to capture the Li lines. For the analysis of O and Li, a fs laser was used for ablation. A high-resolution spectra detection system was used to detect the Li signal and a low-resolution detection one was used to record the O signal. Emissions of single laser shots were recorded and 12 random locations were selected for statistics.

Raman spectra of the pellets were recorded on a "Labram" Raman confocal microscope system (ISA Groupe Horiba) in the backscattering configuration with a 488 nm Argon ion laser (Coherent Inc. Innova 70), and 10x magnification, 0.25 numerical aperture and 22 mm focal length optical objective (Olympus). The laser beam intensity at the sample was adjusted to 0.1 mW for a beam diameter of ça. 2 µm.

X-ray photoelectron spectroscopy (XPS) studies of the polished LLZO pellets were performed using a PHI 5400 XPS system equipped with an Al X-ray source (incident photon energy of 1486.7 eV). XPS samples were sealed in a sample transfer tool under Ar environment. The aperture size was set to 1.1 mm in diameter. The binding energy of the obtained XPS spectra was calibrated with respect to the C 1s peak of adventitious carbon at 284.8 eV. XPS spectra were quantitatively analyzed by deconvoluting Voigt-type line-shapes, preceded by subtracting Shirley-type background (for Zr *3d* spectra) and linear background (for Al *2p* and Li *1s* spectra).

Zr and La K-edge X-ray absorption spectroscopy (XAS) experiments were conducted on LLZO powder samples processed in air and Ar atmospheres at beamline BL 4-1 at Stanford Synchrotron Radiation Lightsource (SSRL), in transmission mode using a Si (220) double crystal monochromator. Edge calibration was performed using Zr (17,988 eV) and La (38,939 eV) standards, each located in front of a reference ion-chamber and measured simultaneously with each spectral sample. All data processing, including normalization was carried out using the software SIXPACK by fitting a linear polynomial to the pre-edge region and a quadratic polynomial to the post-edge region of the absorption spectrum. The energy threshold, E_0 of the reference Zr and La foil was determined from the peak in the first derivative of the spectrum, and all spectra were

linearly calibrated using the difference between the obtained E_0 and the tabulated absorption edge energy for metal K-edge. Pre-edge background subtraction and normalization were carried out. Background removal and edge-step normalization were performed using the Athena module in the Demeter program pack [28]. Ifeffit in Artemis module in the Demeter program pack [28] was then used to fit the EXAFS. The fitting was limited to a k range of 2-10 $Å^{-1}$, dk = 1 $Å^{-1}$ using Hanning windows, R range from 1 to 4 Å.

2.4 Electrochemical Characterization

Metallic lithium was spread on both sides of the sintered LLZO pellets. These pellets were then placed between lithium foil disks on both sides and assembled into a Swagelok-type cell. Physical contacts were maintained by compression of the spring at controlled displacement in the Swagelok cell with an estimated pressure of 200 kPa, derived from considering the spring displacement and spring constant. Samples were assembled in the same Swagelok cell with controlled displacement so that similar pressures were used for each.

AC impedance measurements of the symmetrical Li/LLZO/Li cells were carried out using a VMP3 multichannel potentiostat/galvanostat (Bio-Logic Science Instruments) equipped with a frequency response analyzer.. Impedance data were collected at frequencies from 1 MHz to 1 Hz. Galvanostatic experiments were carried out on symmetrical Li/LLZO/Li cells by passing current through cells for 2 hours and then switching polarity until cell failure occurred.

The partial electronic conductivity was determined using a Hebb-Wagner cell configuration.[28] An Au electrode was sputtered on one side of the LLZO specimen and

a Li non-blocking electrode was applied on the other side. The cell was tested at a constant potential of 2 V and the corresponding current decay was monitored for 12 h to approximate equilibrium conditions.

3. Results and Discussion

Figure 1 shows optical images of LLZO pellets sintered under argon and air. The sample sintered in air has a yellow-brown cast, while the one processed under argon is a grayish-white. These color differences are also seen in the powders used to cover the pellets during the heat treatment; gray for the powder used for processing under Ar, and ivory for that used in air.

Pellets fabricated from attrition-milled LLZO powders heated in air are typically 92-94% dense and have microstructures consisting of very large (~150 μm) and irregularly shaped grains [25]. Figure 2 shows scanning electron micrographs of the two types of pellets, as sintered. The similarities in the microstructures rule this out as a cause of the color differences seen in the pellets. The XRD patterns of polished pellets are presented in Figure 3, along with a calculated reference pattern for a cubic LLZO with a lattice parameter of 12.972 Å for comparison. All reflections in the experimental patterns can be indexed to that of a cubic garnet structure, with no obvious peaks belonging to common impurity phases. Peaks in the pattern of the pellet sintered under argon are broader than those for the pellet sintered in air, and the lattice parameter is slightly larger (12.987 Å for the former and 12.962 Å for the latter). This suggests that there are likely some minor differences in the crystal structures of the two materials. Both the color change and the larger unit cell for the Ar-processed sample suggest that more oxygen vacancies are present than in the air-processed material [29-31].

Figure 4 shows the Arrhenius plot of the total conductivities as a function of temperature of the two kinds of pellets. It was not possible to deconvolute bulk and grain boundary conductivities from the impedance data: see reference [15] for typical Nyquist plots of LLZO samples made in air. Total conductivities of the sample processed under Ar are higher than that of the sample prepared in air at every temperature that was measured. For example, at room temperature, $\sigma \approx 1.3 \times 10^{-4}$ S/cm for LLZO_air, compared to ~4×10^{-4} S/cm for LLZO_Ar. The reported total conductivities of Al-substituted LLZOs vary somewhat depending on processing details and exact composition but typically range from less than 0.1 to 0.5 mS/cm at room temperature [2, 22, 23, 32-34]. The values obtained here for LLZO_air are close to what we have reported before for similarly made samples [25]. The activation energy of LLZO_Ar is approximately 0.31 eV, lower than that of LLZO_air, which was found to be 0.36 eV. Hebb-Wagner measurements show that the leakage electronic current of the pellet prepared under Ar is more than an order of magnitude higher than that of the one processed in air, although these values show that both materials are primarily ionic, not electronic conductors. An estimation of partial electronic conductivity of the Ar and air processed samples, based on Hebb-Wagner cell measurements, are 2.2×10^{-9} S/cm and 1.0×10^{-10} S/cm, respectively. The most likely explanation for the higher partial electronic conductivity of the former is a higher concentration of un-paired electrons associated with small amounts of either charged vacancies or reduced atoms. Because Zr and La are relatively stable and difficult to reduce or move to interstitial positions under the processing conditions used here, we suspect that the Ar annealed samples have higher numbers of oxygen vacancies. A summary of the physical and electrochemical properties of the LLZO pellets is given in

Table 1.

The improvement in electrochemical properties of the Ar-processed material is also observed in a comparison of the DC cycling behaviors of the symmetrical Li/LLZO cells (Figure 5). Voltage instability occurs rapidly when LLZO prepared in air is used as the solid electrolyte in the cell, consistent with our previously reported results on large-grained samples similar to the ones reported here [25]. This behavior has been attributed to the tendency for metallic lithium to deposit in grain boundaries, leading to shorting. In smaller-grained samples, the larger percentage of grain boundaries dissipates the current distribution more effectively, leading to less current focusing and resulting in delayed formation of dendrites and better cycling behavior. Somewhat surprisingly, given the similar microstructures, the cell containing the LLZO prepared under Ar could be cycled for a much longer period of time before failure occurred, and the polarization was lower due to the overall higher conductivity. It is possible that differences in the composition and, consequently, the conductivities of the grain boundaries of the two samples account for the dissimilar behaviors, although little is known at present about their chemistries.

At this point, questions naturally arise as to the origins of the different behavior observed between these two types of samples, given the similarities in structure and microstructure. To answer these questions, extensive physical characterization was carried out to probe for possible chemical, structural, and local environmental differences. LIBS was used to determine the chemical compositions of the two LLZO specimens as a function of sample depth (Figure 6). In both cases, some variation in elemental distribution as a function of depth is observed; in particular there is a slight enrichment of lithium and oxygen content near the surfaces, which may be due to the

presence of Li_2CO_3.[19] The lithium enrichment near the surface is less obvious for the specimen prepared under Ar, although there is slightly higher Li content deeper inside this pellet overall. The average compositions from ICP-OES are $Li_{5.4}Al_{0.3}La_3Zr_{1.95}O_{11.55}$ for the sample made in air and $Li_{5.6}Al_{0.3}La_3Zr_{1.92}O_{11.59}$ for the one made under Ar where elements are normalized to La contents. Note that O content is estimated from charge compensation considerations. The overall compositions of the two materials were not substantially different, within error, although these results suggest that sintering under Ar may have aided in preventing loss of Li during sintering.

Raman spectroscopy was used to obtain further information about the structure of LLZO (Figure 7). For both specimens, Raman spectrum confirmed the cubic structure as Raman peaks at ~260, 360, 410, 515 and 650 cm^{-1} could be assigned to the LLZO cubic phase. Specifically, the peak at 650 cm^{-1} can be tentatively assigned to the Zr-O stretching vibration mode according to Tietz et al. [35]. In an isotope study, Orera et al. [36] suggested that the peak shifts in the 330-600 cm^{-1} region are sensitive to isotope effects in the tetragonal phase LLZO, although shifts for the cubic polymorph are not as sensitive due to the lower Li content in the cubic phase. In this region, we did not observe apparent shifts of the Raman peaks but the relative intensities changed, particularly for the 650 cm^{-1} peak *vs.* the ~360 cm^{-1} peak. We speculate that the relative intensity change could possibly be due to the sensitivity and concentration of Li at sites and Zr at the octahedral sites of the cubic phases. The results are consistent with the Ar-annealed LLZO having higher lithium content, assuming that Zr located in octahedral sites remained the same under these sintering conditions, a reasonable assumption.

Figure 8 shows La 4d and Zr 3d XPS spectra. This technique probes sample

surfaces, and positions of the peaks in these spectra are sensitive to oxidation states and speciation. In some cases, color changes of the material are associated with chemical valence changes, e.g, reduction of metallic elements. During sintering, the LLZO pellets were exposed to either air or Ar atmospheres. The microstructure evolved dynamically when densification occurred during the sintering process. The interiors of the pellets were likely less affected by the environment than the surfaces. Thus, any chemical changes are more likely to be observable on surfaces rather than in the bulk. Comparing surface sensitive XPS and bulk sensitive hard XAS data (Figure 9) is therefore instructive. The XPS data are consistent with what has been reported previously for LLZO materials. La 4d and Zr 3d doublets due to spin-orbital coupling appear around binding energies of 98 − 108 eV and 180-180 eV, respectively as expected for La^{3+} and Zr^{4+} ions, for both samples. Thus, neither Zr nor La were reduced during sintering in Ar at 1100°C, at least to a depth of about 3-5 nm. In the XAS experiment the Zr K-edge appears at ~18 keV and the La K-edge at ~38 keV for both samples, with no noticeable shifting for the sample prepared under Ar.

The Fourier-transformed (FT) EXAFS spectra (k^2 weighted in k-space without phase-corrected FT, resulting in shorter apparent bond lengths in the plots than the real values) at Zr K edges are shown in Figure 10. The first peak at approximately 1.9 Å in is assigned to the scattering path from Zr (16a) to the nearest neighboring oxygen atoms, essentially Zr-O bonds in the octahedral unit. The second peak at about 3.3 A is assigned to Zr next to the nearest metal atoms (La, 24c). The X-ray cross-sections of Li located at interstitial sites are too small to be detected in this experiment. The third peak at ~5.2 A, representing the third shell of nearest atoms, may include multiple scattering paths

involving O and other metal atoms. The Zr-O bond lengths and Zr-La atomic distances and the relative intensities of the first two peaks are not substantially different for the two samples, indicating the degree of ordering in both materials were similar. Likewise, the amplitudes and positions of the third peak were also similar in both cases.

These results indicate that there are only very small differences in the bulk and surface compositions and structures of the two types of samples. The most significant one is a slight compositional variation, which indicates that the bulk of Ar-processed LLZO is slightly more Li-rich and possibly contains more oxygen vacancies than the material processed in air. Differences in grain boundary compositions and conductivities may also be responsible for the observed variations in electrochemical behavior.

4. Conclusions

This study was designed to understand the impact of sintering atmosphere on the structural, chemical, and electrical properties of LLZO solid electrolytes. The electrical properties were improved when LLZO was sintered under Ar compared to when it was sintered in air; namely total conductivity was higher and the cycling behavior was improved. An increase in electronic conductivity was also observed, but both materials are still predominantly ionic conductors. There was no evidence of reduction of Zr or La either in the bulk or on surfaces. The microstructure was not affected by the change in processing atmosphere, but a small expansion of the lattice parameter was observed, consistent with increased numbers of oxygen vacancies. Differences in the grain boundary chemistries and conductivities are also likely and could also account for the dissimilar electrochemical behaviors of the two samples. Our future work is directed

towards a fuller understanding the differences caused by different annealing conditions at atomic scale.

5. References

[1] R Murugan, V Thangadurai, W Weppner (2007) Angewandte Chemie 46: 7778. Doi:10.1002/anie.200701144

[2] V Thangadurai, S Narayanan, D Pinzaru (2014) Chem Soc Rev 43: 4714. Doi:10.1039/c4cs00020j

[3] JB Bates, NJ Dudney, B Neudecker, A Ueda, CD Evans (2000) Solid State Ionics 135: 33.

[4] C Cao, Z-B Li, X-L Wang, X-B Zhao, W-Q Han (2014) Frontiers in Energy Research 2. Doi:10.3389/fenrg.2014.00025

[5] J van den Broek, S Afyon, JLM Rupp (2016) Advanced Energy Materials: 1600736. Doi:10.1002/aenm.201600736

[6] Y Lu, JB Goodenough (2011) Journal of Materials Chemistry 21: 10113. Doi:10.1039/c0jm04222f

[7] EN S. Visco, B. Katz (2007) PolyPlus Battery Company, Berkeley CA, U.S.

[8] CA Geiger, E Alekseev, B Lazic, et al. (2011) Inorganic chemistry 50: 1089. Doi:10.1021/ic101914e

[9] T Thompson, J Wolfenstine, JL Allen, et al. (2014) Journal of Materials Chemistry A 2: 13431. Doi:10.1039/c4ta02099e

[10] D Rettenwander, CA Geiger, M Tribus, P Tropper, G Amthauer (2014) Inorganic chemistry 53: 6264. Doi:10.1021/ic500803h

[11] X Tong, V Thangadurai, ED Wachsman (2015) Inorganic chemistry 54: 3600. Doi:10.1021/acs.inorgchem.5b00184

[12] D Rettenwander, A Welzl, L Cheng, et al. (2015) Inorganic chemistry 54: 10440. Doi:10.1021/acs.inorgchem.5b01895

[13] D Rettenwander, G Redhammer, F Preishuber-Pflugl, et al. (2016) Chemistry of materials : a publication of the American Chemical Society 28: 2384. Doi:10.1021/acs.chemmater.6b00579

[14] D Rettenwander, CA Geiger, G Amthauer (2013) Inorganic chemistry 52: 8005. Doi:10.1021/ic400589u

[15] SR Catarelli, D Lonsdale, L Cheng, J Syzdek, M Doeff (2016) Frontiers in Energy Research 4. Doi:10.3389/fenrg.2016.00014

[16] L Cheng, CH Wu, A Jarry, et al. (2015) ACS applied materials & interfaces 7: 17649. Doi:10.1021/acsami.5b02528

[17] WE Tenhaeff, E Rangasamy, Y Wang, et al. (2014) ChemElectroChem 1: 375. Doi:10.1002/celc.201300022

[18] S Afyon, F Krumeich, JLM Rupp (2015) J. Mater. Chem. A 3: 18636. Doi:10.1039/c5ta03239c

[19] L Cheng, EJ Crumlin, W Chen, et al. (2014) Physical chemistry chemical physics : PCCP 16: 18294. Doi:10.1039/c4cp02921f

[20] A Sharafi, HM Meyer, J Nanda, J Wolfenstine, J Sakamoto (2016) Journal of Power Sources 302: 135. Doi:10.1016/j.jpowsour.2015.10.053

[21] CL Tsai, V Roddatis, CV Chandran, et al. (2016) ACS applied materials & interfaces 8: 10617. Doi:10.1021/acsami.6b00831

[22] E Yi, W Wang, J Kieffer, RM Laine (2016) J. Mater. Chem. A 4: 12947. Doi:10.1039/c6ta04492a

[23] Y Wang, P Yan, J Xiao, X Lu, J-G Zhang, VL Sprenkle (2016) Solid State Ionics 294: 108. Doi:10.1016/j.ssi.2016.06.013

[24] Y Ren, H Deng, R Chen, Y Shen, Y Lin, C-W Nan (2015) Journal of the European Ceramic Society 35: 561. Doi:10.1016/j.jeurceramsoc.2014.09.007

[25] L Cheng, JS Park, H Hou, et al. (2014) J. Mater. Chem. A 2: 172. Doi:10.1039/c3ta13999a

[26] Y Li, Z Wang, C Li, Y Cao, X Guo (2014) Journal of Power Sources 248: 642. Doi:10.1016/j.jpowsour.2013.09.140

[27] M Kotobuki, K Kanamura, Y Sato, K Yamamoto, T Yoshida (2012) Journal of Power Sources 199: 346. Doi:10.1016/j.jpowsour.2011.10.060

[28] W Weppner, RA Huggins (1978) Ann. Rev. Mater. Sci. 8: 269.

[29] S Mukhopadhyay, T Thompson, J Sakamoto, et al. (2015) Chemistry of Materials 27: 3658. Doi:10.1021/acs.chemmater.5b00362

[30] M Nyman, TM Alam, SK McIntyre, GC Bleier, D Ingersoll (2010) Chemistry of Materials 22: 5401. Doi:10.1021/cm101438x

[31] J Wolfenstine, JL Allen, J Read, J Sakamoto (2013) Journal of Materials Science 48: 5846. Doi:10.1007/s10853-013-7380-z

[32] Y Jin, PJ McGinn (2011) Journal of Power Sources 196: 8683. Doi:10.1016/j.jpowsour.2011.05.065

[33] AA Hubaud, DJ Schroeder, B Key, BJ Ingram, F Dogan, JT Vaughey (2013) Journal of Materials Chemistry A 1: 8813. Doi:10.1039/c3ta11338h

[34] M Amores, TE Ashton, PJ Baker, EJ Cussen, SA Corr (2016) J. Mater. Chem. A 4: 1729. Doi:10.1039/c5ta08107f

[35] F Tietz, T Wegener, MT Gerhards, M Giarola, G Mariotto (2013) Solid State Ionics 230: 77. Doi:10.1016/j.ssi.2012.10.021

[36] G Larraz, A Orera, ML Sanjuán (2013) Journal of Materials Chemistry A 1: 11419. Doi:10.1039/c3ta11996c

Tables

Table 1. Properties of LLZO pellets.

Sample	Sintering conditions	Color	Lattice parameter, Å	σ_{RT}, ionic, S/cm	σ_{RT}, electronic, S/cm
LLZO_air	Air, 1100ºC	Ivory/brown	12.962(7)	1.0×10^{-4}	1.0×10^{-10} S/cm
LLZO_Ar	Ar, 1100ºC	White/gray	12.987(9)	3.0×10^{-4}	2.2×10^{-9} S/cm

Figure Captions

Figure 1. Photographic images of LLZO pellets processed under Ar (top left) and in air (top right), and mother powders used to cover the pellets during thermal processing under Ar (bottom left) and air (bottom right).

Figure 2. SEM images of pellets processed under argon (a) and in air (b).

Figure 3. XRD patterns of LLZO pellets sintered under argon and in air. A reference pattern for cubic LLZO is provided at the bottom.

Figure 4. Arrhenius plot of total conductivities as a function of temperature for LLZO processed in air, and under Ar.

Figure 5. Galvanostatic (DC) cycling of Li/LLZO/Li cells.

Figure 6. Compositions of LLZO_air and LLZO_Ar specimens as a function of sample depth, as determined by LIBS.

Figure 7. Raman spectra of LLZO_air and LLZO_Ar samples. Arrows mark areas of major spectral shifts.

Figure 8. XPS data for LLZO_air and LLZO_Ar samples.

Figure 9. Zr and La K-edge XAS data.

Figure 10. Radial distances (Å) determined from EXAFS data obtained on LLZO_air and LLZO_Ar samples.

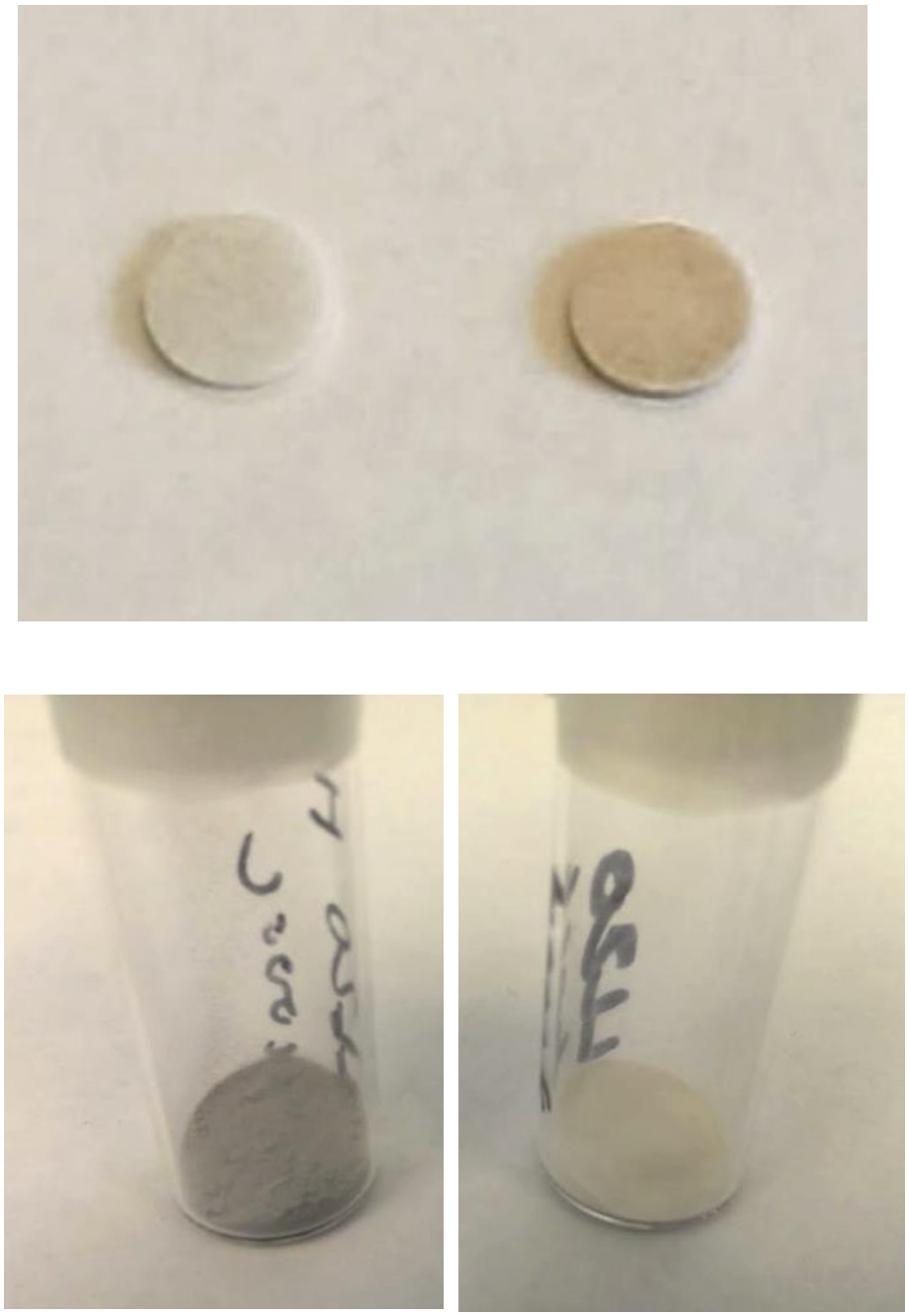

Figure 1.

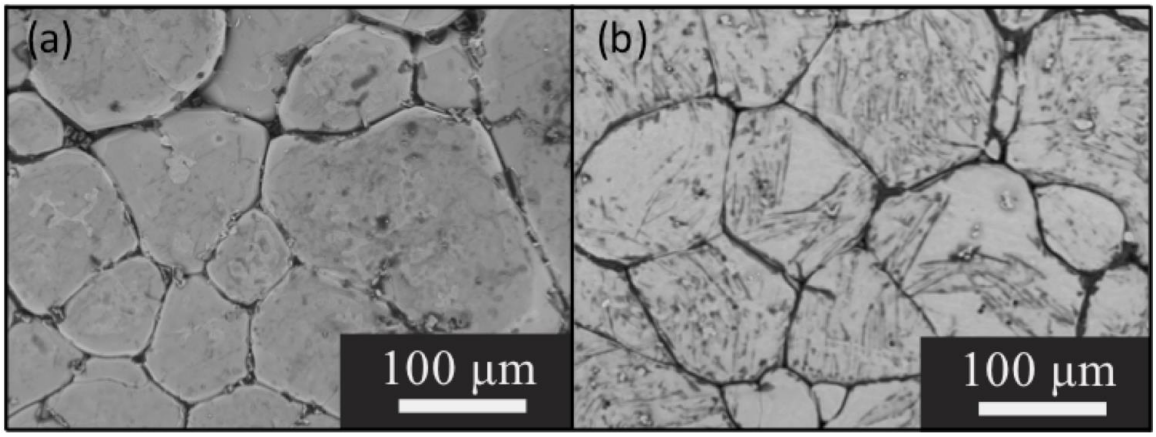

Figure 2

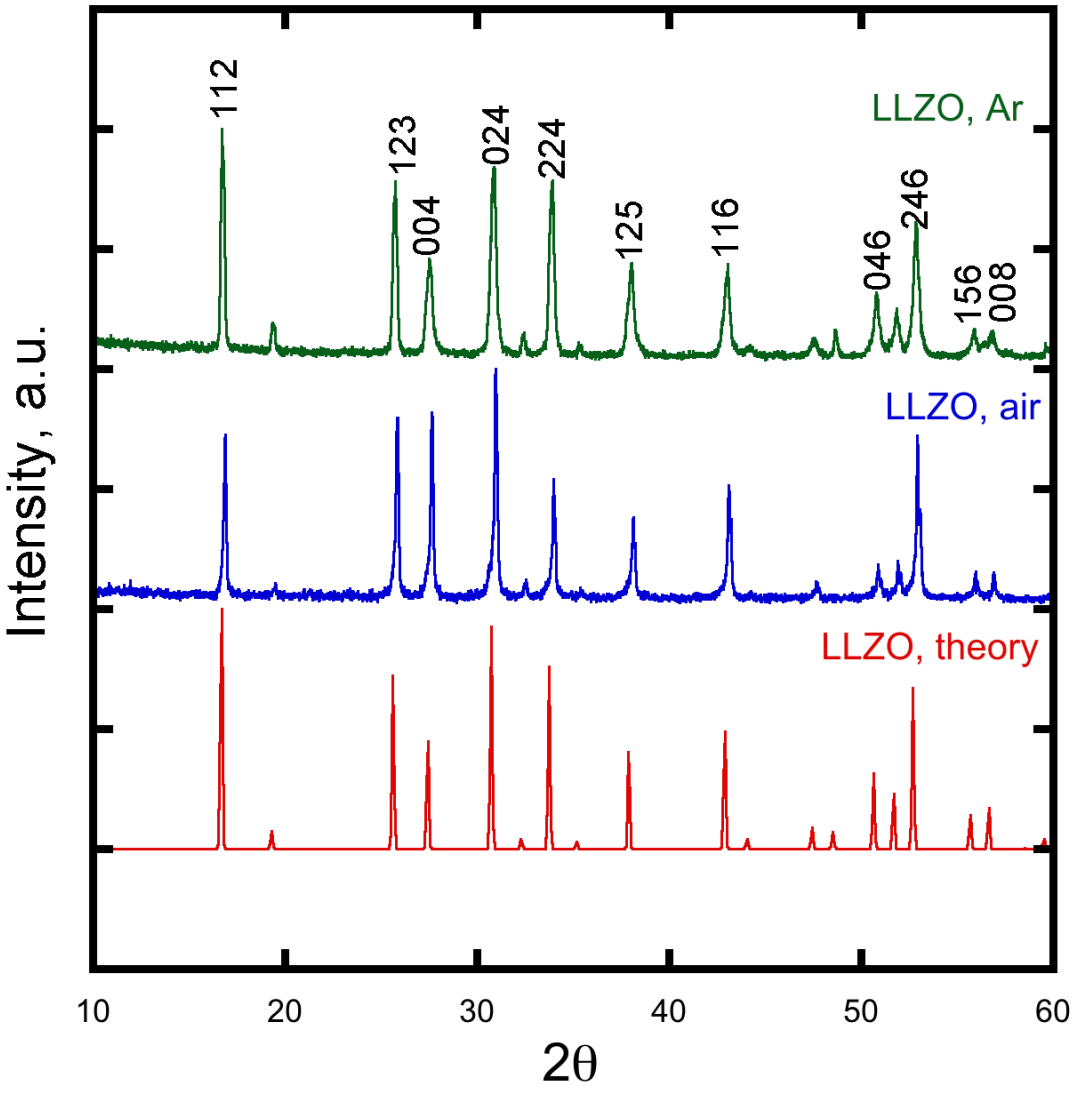
112
123
004
024
224
125
116
046
246
156
008
LLZO, Ar
LLZO, air
LLZO, theory
Intensity, a.u.
10
20
30
40
50
60
2θ

Figure 3

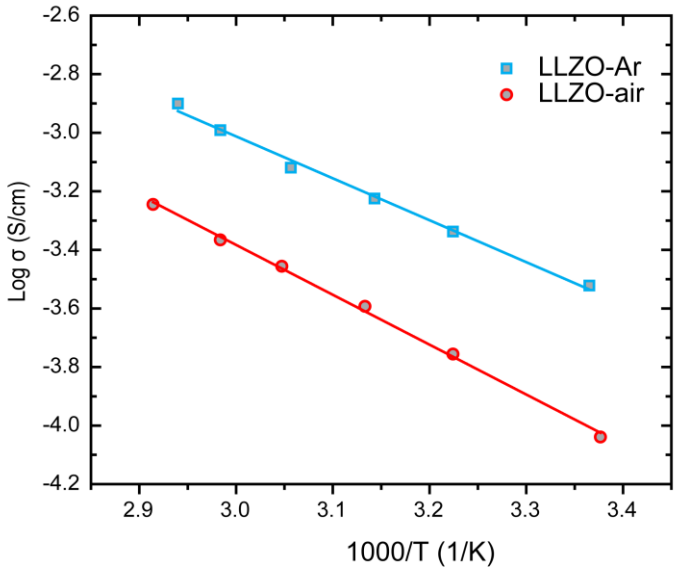
LLZO-Ar
LLZO-air
Log σ (S/cm)
1000/T (1/K)
-2.6
-2.8
-3.0
-3.2
-3.4
-3.6
-3.8
-4.0
-4.2
2.9
3.0
3.1
3.2
3.3
3.4

Figure 4.

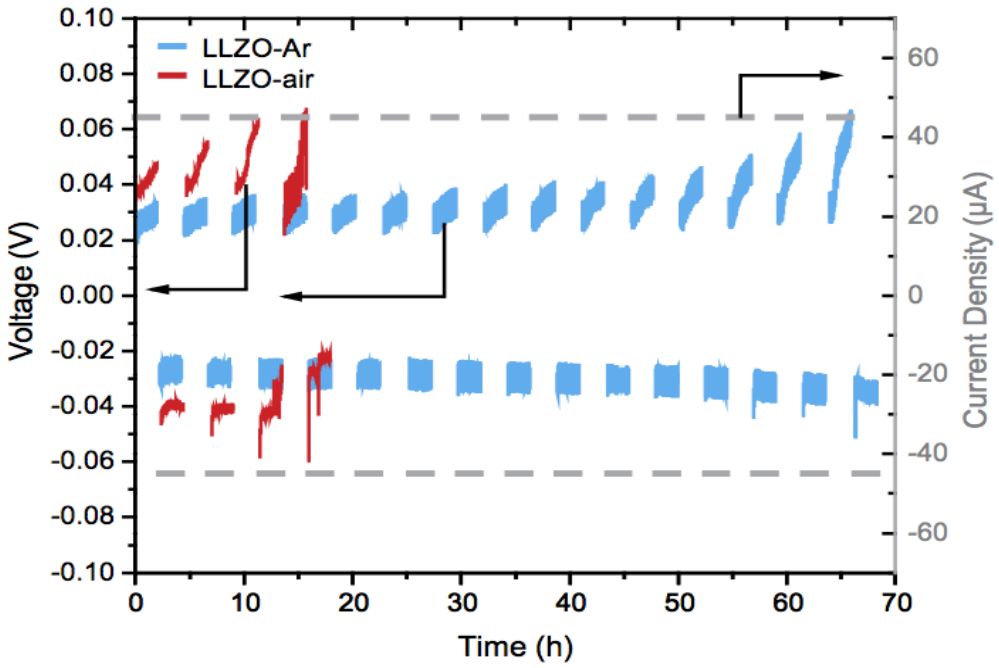
LLZO-Ar
LLZO-air
Voltage (V)
Current Density (μA)
Time (h)
0.10
0.08
0.06
0.04
0.02
0.00
-0.02
-0.04
-0.06
-0.08
-0.10
60
40
20
0
-20
-40
-60
0
10
20
30
40
50
60
70

Figure 5

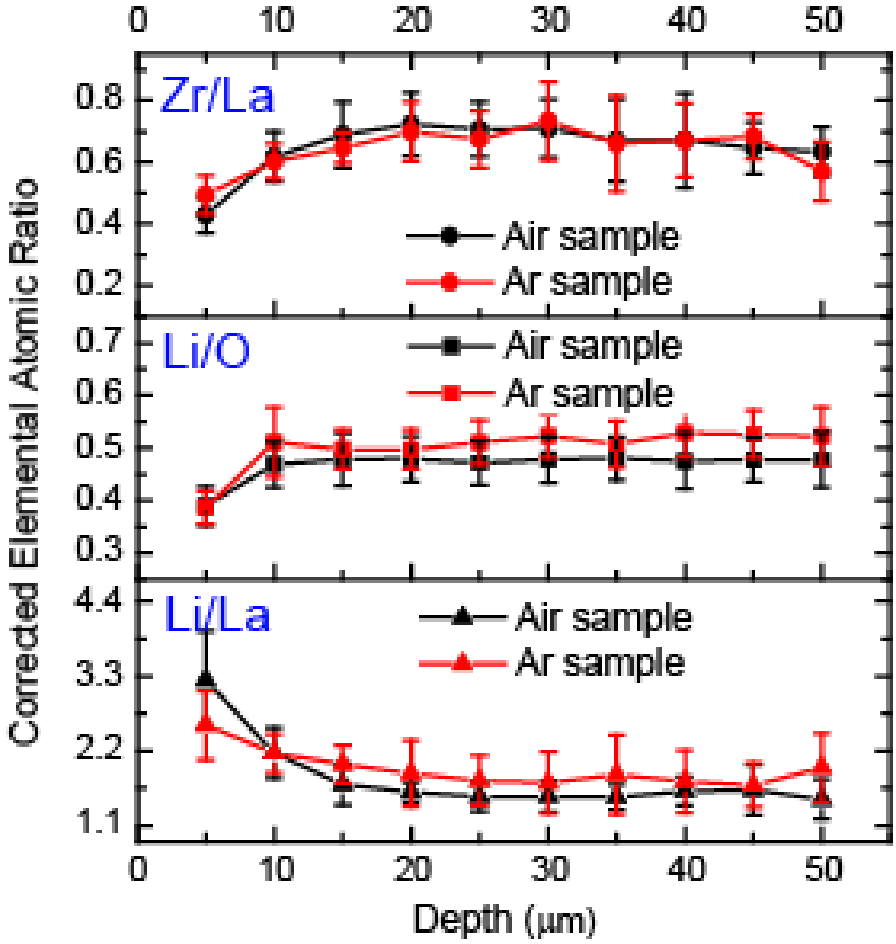
Zr/La
Li/O
Li/La
Air sample
Ar sample
Corrected Elemental Atomic Ratio
Depth (μm)
0
10
20
30
40
50
0.8
0.6
0.4
0.2
0.7
0.5
0.3
4.4
3.3
2.2
1.1

Figure 6.

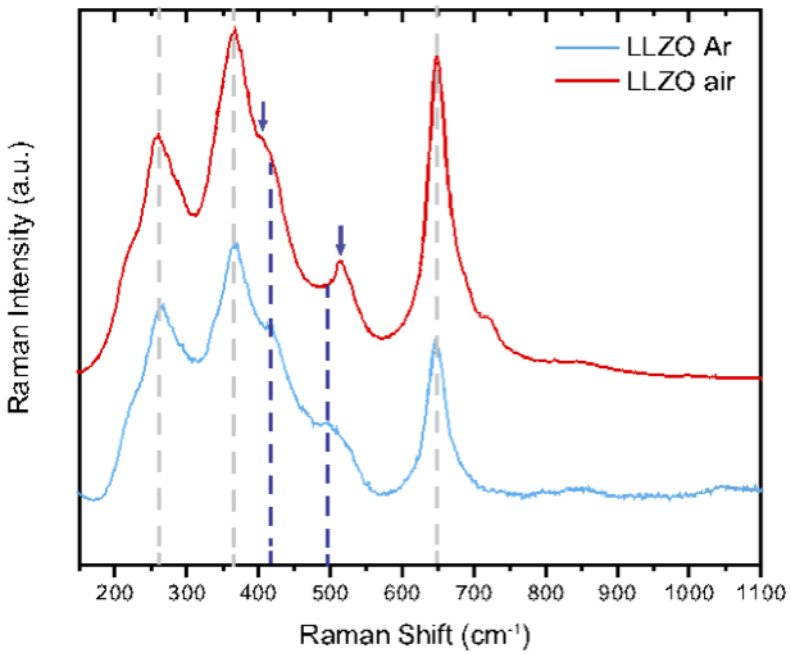
LLZO Ar
LLZO air
Raman Intensity (a.u.)
200
300
400
500
600
700
800
900
1000
1100
Raman Shift (cm-1)

Figure 7

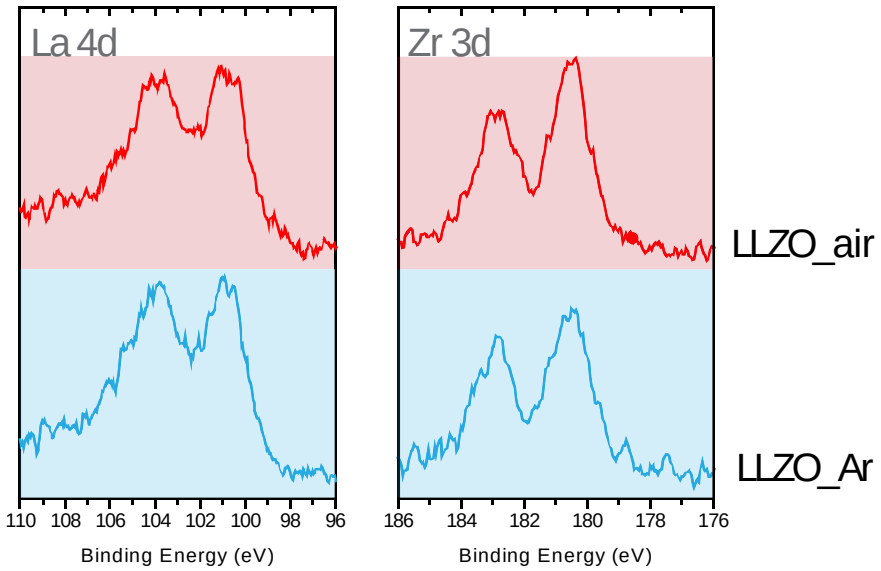
La 4d
Zr 3d
LLZO_air
LLZO_Ar
110 108 106 104 102 100 98 96
Binding Energy (eV)
186 184 182 180 178 176
Binding Energy (eV)

Figure 8

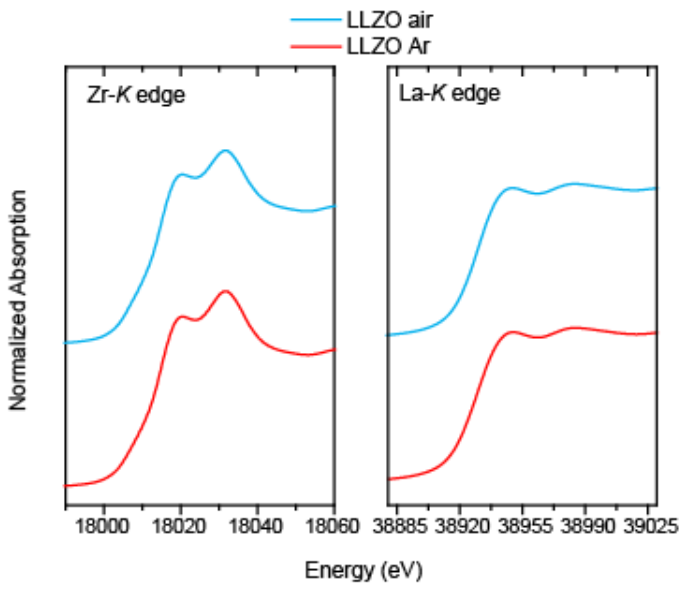
LLZO air
LLZO Ar
Zr-K edge
La-K edge
Normalized Absorption
18000
18020
18040
18060
38885
38920
38955
38990
39025
Energy (eV)

Figure 9.

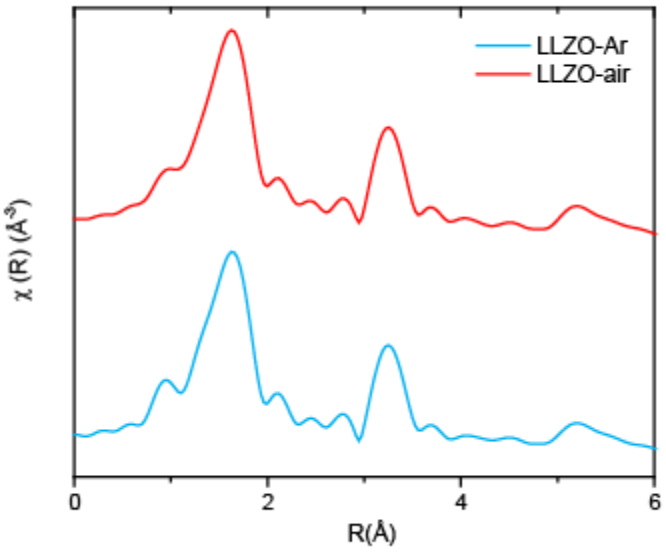

Figure 10.

ERNEST ORLANDO LAWRENCE BERKELEY NATIONAL LABORATORY
Energy Storage and Distributed Resources Division
MS 62R0247/Bldg 62
1 Cyclotron Road
Berkeley, CA 94720
Tel: (510) 486-5821 Fax: (510) 486-4881

2/15/2017

Dear Editor;

We are submitting a revised version of the paper "Enhanced Lithium Ion Transport In Garnet-type Solid Electrolytes" to the journal. We have highlighted changes to the paper in yellow and included a brief "comments to the reviewers" page to explain these. The reviewer's requests were quite reasonable and we made all the changes that were suggested. We hope that the manuscript is now ready for publication in the Journal of Electroceramics.

Sincerely,

Marca M. Doeff
Staff Scientist
Energy Storage and Distributed Resources Division
Lawrence Berkeley National Laboratory
1 Cyclotron Rd, Berkeley, CA 94720
510-486-5821
mmdoeff@lbl.gov